

## REVIEW ARTICLE

# Skeletal muscle dispersion (400-1000 nm) and kinetics at optical clearing

Luís M. Oliveira<sup>1,2,3\*</sup> | Maria I. Carvalho<sup>4</sup> | Elisabete M. Nogueira<sup>1,3</sup> | Valery V. Tuchin<sup>5,6,7</sup>

<sup>1</sup>Physics Department – Polytechnic Institute of Porto, School of Engineering, Porto, Portugal

<sup>2</sup>School of Engineering, Porto University, Porto, Portugal

<sup>3</sup>Centre of Innovation in Engineering and Industrial Technology (CIETI), School of Engineering, Polytechnic of Porto, Porto, Portugal

<sup>4</sup>DEEC and INESC TEC, Faculty of Engineering, University of Porto, Porto, Portugal

<sup>5</sup>Research-Educational Institute of Optics and Biophotonics, Saratov National Research State University, Saratov, Russia

<sup>6</sup>Laboratory of Laser Diagnostics of Technical and Living Systems, Institute of Precision Mechanics and Control RAS, Saratov, Russia

<sup>7</sup>Laboratory of Femtomedicine, ITMO University, St. Petersburg, Russia

**\*Correspondence**

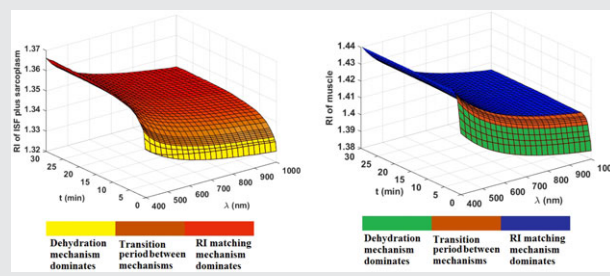
Luís M. Oliveira, Physics Department – Polytechnic Institute of Porto, School of Engineering, Porto, Portugal.  
Email: lmo@isep.ipp.pt

Skeletal muscle dispersion and optical clearing (OC) kinetics were studied experimentally to prove the existence of the refractive index (RI) matching mechanism of OC. Sample thickness and collimated

transmittance spectra were measured during treatments with glucose (40%) and ethylene glycol (EG; 99%) solutions and used to obtain the time dependence of the RI of tissue fluids based on the proposed theoretical model. Calculated results demonstrated an increase of RI of tissue fluids and consequently proved the occurrence of the RI matching mechanism. The RI increase was observed for the wavelength range between 400 and 1000 nm and for the 2 probing molecules explored. We found that for 30 min treatment with 40% glucose and 99% EG, RI of sarcoplasm plus interstitial fluid was increased at 800 nm from 1.328 to 1.348 and from 1.328 to 1.369, respectively.

**KEYWORDS**

optical clearing, refractive index, refractive index matching, skeletal muscle



## 1 | INTRODUCTION

Soft biological tissues, in general, have a heterogeneous composition, with cell organelles, proteins and fibers (considered as scatterers) distributed through a liquid ground substance, commonly designated by cell cytoplasm and interstitial fluid (ISF). ISF contains mainly water and some dissolved salts and organic compounds [1–3]. The scatterers have a higher refractive index (RI) than ISF, and since no noticeable physical boundaries between tissue components are seen on a macroscopic scale, tissues can be described as a continuous structure with spatial variations in the RI [1]. At 589.6 nm, the RI of ISF usually ranges between 1.35 and 1.37, while scatterers present higher values typically between 1.39 and 1.47, or even as high as 1.58 for dry muscle proteins [2] or 1.6 for skin melanin [1].

The RI mismatch between tissue components is the basis of the high light scattering properties that characterize

biological tissues [1, 4–8]. One way to reduce the light scattering is to perform optical clearing (OC) treatment [1]. This treatment reduces light scattering through 2 main mechanisms—tissue dehydration and RI matching [9]. When ex vivo tissue samples are immersed in an OC solution, the osmotic pressure created by the OC agent (OCA) over the tissue, forces water in the ISF to flow out (dehydration mechanism) and the scatterers approach each other (tissue shrinkage) leading to a short-time scattering coefficient ( $\mu_s$ ) increase. In spite of some elevation of the  $\mu_s$ , due to less sample thickness and better ordering (packing) of the scatterers, optical transmittance increases. As the water flows out from the tissue, the OCA in the immersion solution finds it easier to flow in and it will partially replace the water in the cytoplasm and ISF, forcing the scatterers to separate from each other (tissue swelling) once again. Common OCAs used in these treatments are glucose, glycerol or dimethyl sulfoxide, which have RI values greater than water

and more approximated to the high RI values of tissue scatterers [10]. As OCAs flow into the cytoplasm and ISF, the RI matching mechanism occurs, leading to a decrease in light scattering [9]. Although this mechanism is commonly accepted, it has never been experimentally proven. However, an alternative indirect method to evaluate the kinetics of the RI of the interstitial space of tissues  $n_0(t)$  based on the reconstruction of temporal behavior of the scattering coefficient  $\mu_s(t)$  from measurements of the collimated transmittance ( $T_c$ ) of a tissue sample during OC can be proposed [1, 11]. To perform a more accurate calculation of  $n_0(t)$ , temporal measurements of sample thickness should also be provided during OC, because OCA induces tissue shrinkage or swelling. Therefore, considering the relation between  $n_0(t)$  and  $\mu_s(t)$ , we have performed thickness and  $T_c$  measurements from skeletal muscle samples during treatments with 40% glucose and 99% ethylene glycol (EG) to evaluate the kinetics of the RI of the interstitial space of the muscle. Glucose and EG are 2 different molecules that were used as independent OCA examples for tissue probing and method validation. In this study, we are presenting the calculation method and corresponding algorithm to obtain the natural dispersion curve of skeletal muscle and its kinetics during OC (section 2) and the sequential results from these calculations for the 2 OCAs studied (section 3).

## 2 | MATERIALS AND METHODS

### 2.1 | Method of RI quantification

An indirect method to evaluate the kinetics of the RI of the interstitial space of tissues during OC is described in the literature [1]. Considering a simple approximation, where the diffusion of an OCA with low osmotic pressure into the interstitial space does not affect density or the physical dimensions of tissue scatterers, it is possible to describe the change in the  $\mu_s$  of the tissue as a function only of the change of the RI of the interstitial space. Equation (1) shows this change in  $\mu_s$  for a particular time  $t$  of treatment [1]:

$$\mu_s(t) = \mu_s(t=0) \times \frac{\left[\frac{n_s}{n_0(t)} - 1\right]^2}{\left[\frac{n_s}{n_0(t=0)} - 1\right]^2}. \quad (1)$$

In Eq. (1),  $\mu_s$  is calculated at any time  $t$  of treatment as a function of the value of  $\mu_s$  from the natural tissue ( $\mu_s(t=0)$ ), the RI of the scatterers ( $n_s$ ), the RI of the interstitial space for the natural tissue ( $n_0(t=0)$ ) and the RI of the interstitial space at time  $t$  ( $n_0(t)$ ) [1].

Since  $n_s$  is assumed to remain unchanged during treatment, Eq. (1) establishes a relation between  $\mu_s(t)$  and  $n_0(t)$  and it can be solved to obtain  $n_0(t)$  from  $\mu_s(t)$ .

In reality, an OCA with a high osmotic pressure will also interact with tissue components and consequently, tissue shrinkage or swelling might also take place. For slab-form tissue samples under OC treatment, the superficial area of the sample is usually much larger than sample thickness. Consequently, sample volume variations can be calculated directly from thickness measurements made during OC. Such variations must be taken into account in Eq. (1) to perform a correct calculation.

Considering the relation between  $n_0(t)$  and  $\mu_s(t)$  indicated in Eq. (1), we have performed thickness and  $T_c$  measurements from skeletal muscle samples during treatments with 40% glucose and 99% EG to evaluate the kinetics of the RI of the interstitial space of the muscle.

### 2.2 | Experimental studies

Skeletal muscle samples from Wistar Han rats were used to perform thickness and  $T_c$  measurements considered in this research. All muscle samples used in measurements were previously sliced with a cryostat (model HM560 from Thermo Scientific, Waltham, Massachusetts) with 0.5 mm thickness.

The experimental setups used to perform these measurements are presented in Figure 1.

Considering the  $T_c$  measuring setup presented in Figure 1A, a halogen lamp (HL-2000 model from Avantes,

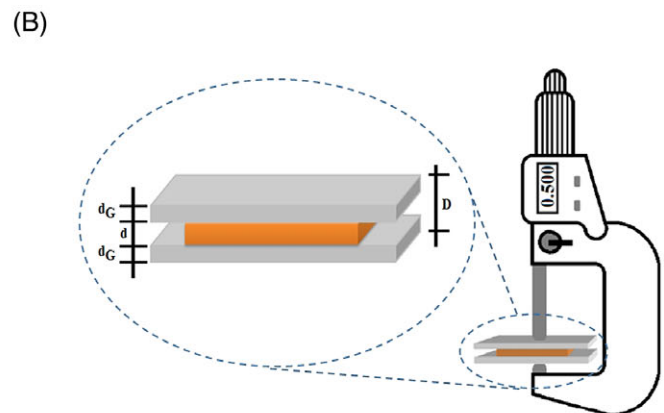
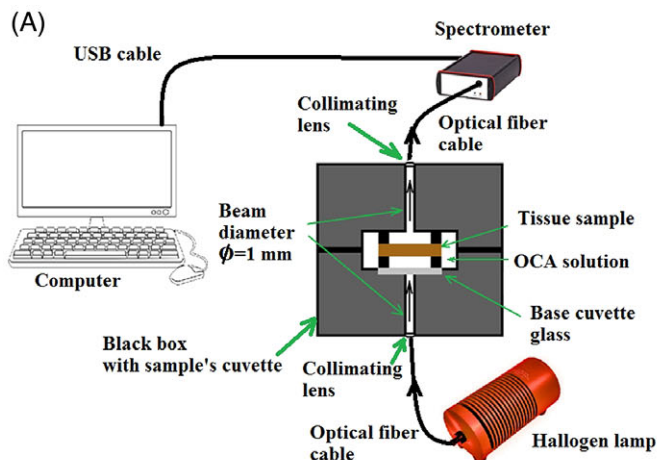


FIGURE 1 (A)  $T_c$  measuring setup and (B) thickness measuring setup

Apeldoorn, The Netherlands) was used to illuminate the tissue sample. The transmitted spectra were collected by an Avantes spectrometer (AvaSpec-2048-USB2 model) configured to measure between 200 and 1000 nm with 1 nm resolution. Since the halogen lamp power is very low below 400 nm, we have considered spectra between 400 and 1000 nm in this research. The black box that contains the sample's cuvette was constructed to guarantee a collimated beam with 1 mm in diameter before and after the sample. This setup was used to measure spectra from the natural samples and during OC treatments. We have performed 3 sets of measurements for treatments with 40% glucose and other 3 for treatments with 99% EG. Although spectra were acquired with a time resolution of 1 seconds during OC treatments, not all were used in calculations, as indicated in section 3.

Thickness measurements were made using the setup presented in Figure 1B. The muscle slices were introduced between 2 microscope glasses with known thickness ( $d_G$ ). A micrometer with a measurement precision of 0.001 mm was used to measure the global thickness of this setup ( $D$ ), and the sample thickness was calculated as  $d = D - 2 \times d_G$ . After measuring the thickness of the natural sample, the OC solution (40% glucose or 99% EG) was injected in-between the 2 microscope glasses and thickness measurements were taken at each 15 seconds until 2 minutes of treatment and at each min after that. These measurements were made in a very gentle way to avoid excessive tissue compression and obtain thickness values as true as possible. Three sets of measurements were made for treatments with 40% glucose and other 3 were made for treatments with 99% EG [12] to calculate the average time dependence for sample thickness [9].

### 2.3 | Muscle's dispersion between 400 and 1000 nm

Skeletal muscle is a soft fibrous tissue with a heterogeneous composition. The skeletal muscle can be described as a collection of muscle cells that are distributed through the ISF. The muscle cells contain protein fiber chains (actin and myosin) that are hydrated by another liquid—the sarcoplasm. Like the ISF, the sarcoplasm contains mainly water and a small quantity of dissolved salts, minerals and proteins [13]. Such composition for the muscle indicates that a significant RI mismatch exists between the proteins (RI  $\sim 1.53$ ) and the muscle fluids (RI  $\sim 1.35$ ). Such mismatch is responsible for strong light scattering inside the muscle in the UV-near infrared (NIR) range [1, 4, 6–8, 14–20], which will originate significant power loss in a light beam or low contrast images obtained from small tissue depths [21, 22].

A simplistic model can be considered to estimate the natural dispersion curve of the muscle, where only 2 tissue components are considered: the scatterers (dried proteins, salts and minerals) and water. By knowing the wavelength dependence of the RI of water and scatterers and the

correspondent volume fractions (VFs), the calculation of the dispersion curve of the muscle can be made using the Gladstone and Dale law of mixtures [1, 23–26]:

$$\begin{aligned} n_{\text{sample}}(\lambda) &= n_{\text{water}}(\lambda)f_{\text{water}} + n_{\text{scatterer}}(\lambda)f_{\text{scatterer}}, \\ f_{\text{water}} + f_{\text{scatterer}} &= 1 \end{aligned} \quad (2)$$

In Eq. (2),  $n_{\text{water}}(\lambda)$  represents the wavelength dependence of the RI of water,  $n_{\text{scatterer}}(\lambda)$  is the wavelength dependence of the RI of scatterers and  $f_{\text{water}}$  and  $f_{\text{scatterer}}$  represent the VFs for water and scatterers, respectively.

The VF of water in the skeletal muscle from rat is reported in the literature as  $0.756 \pm 0.003$  [27]. This value indicates that the VF for scatterers in our model is  $0.244 \pm 0.003$ . Reinoso et al. [27] have also indicated other values for the VF of water that are as low as 0.710 or as high as 0.761. This means that the water content in muscle tissues depends on the samples used in study and conditions of measurements performed. Since we have used skeletal muscle from the Wistar Han rat in our studies, we need to estimate the appropriate water content for this muscle.

The wavelength dependence for the RI of water is also reported in the literature for a few temperatures [28]. Since we have performed our measurements at 20°C and considered the wavelength band between 400 and 1000 nm, we will consider water dispersion in this band as collected from Ref. [28] for that temperature. The wavelength dependence for the RI of scatterers is not known.

In our early stage research, we have used a single-wavelength Abbe refractometer to measure the RI of muscle at 589.6 nm. Measuring from several samples, we obtained a mean RI of  $1.398 \pm 0.005$ . We have also measured from samples in different stages of dehydration to estimate for maximally achieved dehydration in the experiment the RI of the scatterers as  $1.584 \pm 0.025$  at this wavelength [2].

Considering the reference wavelength of 589.6 nm, we can use these values and the RI of water from Ref. [28] (1.333) in Eq. (2) to estimate the VFs for water and scatterers. Performing these calculations, we have estimated these VFs for the rat skeletal muscle:  $f_{\text{water}} = 0.741$  and  $f_{\text{scatterer}} = 0.259$ .

Using these values for  $\lambda = 589.6$  nm, we have adopted a particular calculation procedure to estimate the dispersion curve for the skeletal muscle. Bolin et al. [29] report the RI values of normal bovine skeletal muscle for some wavelengths within the range of 400 to 700 nm. Since bovine and rat skeletal muscles have the same type of proteins—actin and myosin, we can combine our experimental RI data with the data of Ref. [29] to calculate the dispersion curve for the scatterers in rat muscle as already made for other tissues [30]. However, since the published bovine data [29] are only for wavelengths between 400 and 700 nm and for normally hydrated conditions, we need to extrapolate these data to 1000 nm and to dry state.

To perform such extrapolation, the RI data for bovine muscle in Ref. [29] should be fitted with a curve described

by Eq. (3). Such equation is presented in the literature as adequate to fit RI data of skeletal muscle samples for a wider spectral range [31]:

$$n_{\text{bovine-muscle}}(\lambda) = \frac{A}{\lambda^B} + C \quad (3)$$

The parameters A, B and C in Eq. (3) are estimated when the fitting of bovine muscle data is done. The wavelength in this equation is to be used in nanometers. By applying this equation to a spectral range between 400 and 1000 nm, we obtain the dispersion curve for bovine muscle that will be used in the following calculations.

To obtain the dispersion of the scatterers from bovine muscle data to use in rat muscle, we need to subtract the water contribution in bovine muscle to its dispersion curve. For this calculation, it is necessary to know the water VF in bovine muscle. Literature reports that bovine muscle can have water content between 0.709 and 0.741 [32]. Using Eq. (3) after estimating A, B and C, we calculated the RI of bovine muscle at 589.6 nm as 1.400. For the same wavelength, water has an RI of 1.333 [28]. Using these values and the RI of 1.584 for dry proteins [2] in Eq. (4), we calculated the VF of water ( $f_{\text{bovine-water}}$ ) in bovine muscle as 0.734.

$$n_{\text{proteins}}(\lambda) = \frac{n_{\text{bovine-muscle}}(\lambda) - f_{\text{bovine-water}} \times n_{\text{water}}(\lambda)}{1 - f_{\text{bovine-water}}} \quad (4)$$

Having obtained the water VF in bovine muscle, we used Eq. (4) again to subtract the water contribution and obtain the wavelength dependence of the RI of dry proteins. Such wavelength dependence for the RI of proteins was then used in Eq. (2) to reconstruct the wavelength dependence of the RI of rat muscle. The calculated RI value for the skeletal muscle at 589.6 nm was 1.398, as expected. The graphs obtained in the sequential steps of these calculations are presented in section 3 along with the final muscle dispersion curve.

## 2.4 | Muscle's dispersion kinetics during OC

After estimating the dispersion curve for rat skeletal muscle, we wanted to know how its time dependence behaves during OC treatments. We also wanted to evaluate the dispersion kinetics for the RI of the interstitial space to experimentally prove the occurrence of the RI matching mechanism during OC. As indicated in section 2.1, if thickness and  $T_c$  measurements are made during OC treatments, it is possible to calculate the time dependence for the RI of the interstitial space. We have performed those measurements during the treatments with 40% glucose and 99% EG (measurements and time dependencies presented in Refs. [12, 33, 34]). Such measurements have already allowed the estimation of the diffusion properties of glucose [34] and EG [12] in the muscle and can now be used to calculate the RI dispersion kinetics of the tissue under treatment and demonstrate the predicted

increase in the RI of the ISF plus sarcoplasm and of the tissue as a whole.

The simplistic model used to estimate the dispersion curve of the natural skeletal muscle is not adequate to estimate its kinetics during OC. In this case, we have to consider a more realistic tissue model that contains free and bound water. Literature explains the difference between these types of water in tissues: bound water is tightly connected to the other tissue components and can only turn free and move inside the tissues if a strong or long-term stimulation is applied [35]. Both the ISF and sarcoplasm in skeletal muscle contain free and bound water according to Ref. [13]. The bound water in sarcoplasm is bound to the protein fiber chains (myofibrils), providing their hydration and the bound water in ISF is bound to the proteins that are dissolved or to the outside of the muscle cells.

Considering a short-time duration treatment as we did (30 minutes), the only water involved in the fluid exchange with the treating solution will be free water [1, 36]. For this reason, we have to consider hydrated proteins as the scatterers and the free water in ISF plus sarcoplasm as the background fluid that will be able to flow out during treatment.

According to the literature [37], hydrated proteins in skeletal muscle should have an RI of 1.53 at 589.6 nm. Equation (2) was used to obtain the VFs of water and dry proteins that match the reported value of hydrated proteins at 589.6 nm. After obtaining these VF values, the scatterers' dispersion was calculated according to Eq. (5):

$$n_{\text{scatterers}}(\lambda) = 0.785 \times n_{\text{dry proteins}}(\lambda) + 0.215 \times n_{\text{water}}(\lambda) \quad (5)$$

Equation (5) describes the dispersion curve of the scatterers in the skeletal muscle, which will remain unchanged during treatment. The next step consists on determining how the RI of ISF plus sarcoplasm changes during treatment.

Considering a slab-form tissue sample under treatment with a particular OCA, the  $T_c$  measurement made at a particular time of the treatment is a function of the sample thickness and the sample's attenuation coefficient, as described by the Lambert-Beer equation: [4]

$$T_c = \frac{I}{I_0} = e^{(-\mu_t \times d)}. \quad (6)$$

In Eq. (6),  $I$  represents the light intensity measured after transmission through the slab sample,  $I_0$  represents the light reference intensity,  $\mu_t = \mu_a + \mu_s$  is the attenuation coefficient of the sample and  $d$  represents the thickness of the slab sample. For tissues that have a high  $\mu_s$  when compared with  $\mu_a$  (various examples can be found in Table 18 of Ref. [1]), the variations in  $\mu_a$  during OC will be neglectable when compared to the variations in  $\mu_s$  [1]. Note that the explanation for this fact can be found in the nature of the 2 processes taking place during the treatment—tissue loses some water due to the dehydration mechanism and acquires OCA that provides the RI matching mechanism. Water shows no

strong absorption bands for visible and NIR wavelengths. On the other hand, it presents 2 small magnitude absorption bands at 980 and 1190 nm and a high magnitude absorption band at 1450 nm [38]. Moreover, OCAs have their own absorption spectra, but usually they do not have strong absorption bands for visible and NIR wavelengths [1].

Considering thickness and  $T_c$  measurements made during the OC treatment and considering that  $\mu_a$  remains unchanged, the time dependence for  $\mu_s$  can be calculated with a rearranged Beer-Lambert equation:

$$\mu_s(t) = -\frac{\ln[T_c(t)]}{d(t)} - \mu_a, \quad (7)$$

where both  $T_c$  and slab thickness are time dependent during treatment. As indicated in Ref. [1], the significant changes during the treatment occur in the interstitial space due to the liquid fluxes between the tissue and the immersion solution. Such liquid exchange between the tissue and the treating solution will originate changes in RI of the interstitial space and in the VFs of tissue components. By changing the VFs, the scatterer density ( $\rho_s$ ) will also change, and since  $\mu_s$  is the product between the scattering cross section ( $\sigma_s$ ) and  $\rho_s$  [4], the following equation must be considered to determine the time dependence of the RI of the tissue fluids:

$$\bar{n}_0(t) = \frac{n_s}{\left(\sqrt{\frac{\mu_s(t) \times d(t)}{\mu_s(t=0) \times d(t=0)}} \times \left(\frac{n_s}{n_0(t=0)} - 1\right) + 1\right)}. \quad (8)$$

Equation (8), which is a rearranged version of Eq. (1), is a corrected version of the relation between the time dependence of the RI of interstitial space of tissue and the time dependence of  $\mu_s$  of tissue that is presented in Ref. [1], where the scatterer density change was accounted for. The sample thickness for the natural tissue ( $d(t=0)$ ) and its time dependence during treatment ( $d(t)$ ) were introduced in Eq. (8) to account for the scatterer density change. A detailed discussion about this correction is presented in Ref. [39]. In this equation, the RI of the interstitial space of the natural tissue ( $n_0(t=0)$ ) represents the RI of water according to our model.

Considering that during OC only water and OCA fluxes will occur between the interstitial space of the tissue and the immersing solution, we can use thickness and  $T_c$  measurements to perform calculations with Eqs. (7) and (8) and obtain the time dependence for the mean ISF dispersion curve.

For a particular time of treatment, the dispersion curve for the muscle tissue can be calculated from the dispersion curves of the interstitial space ( $\bar{n}_0(\lambda, t)$ ) and scatterers ( $n_s(\lambda)$ ) using Eq. (9):

$$n_{\text{sample}}(\lambda, t) = \bar{n}_0(\lambda, t)f_0(t) + n_s(\lambda)f_s(t), \quad (9)$$

$$f_0(t) + f_s(t) = 1$$

where the appropriate VFs at that particular time of treatment ( $t$ ) are used. These VFs will also change during

treatment due to water content decrease, OCA content increase and volume variation for the sample under treatment. The time dependence for the VFs can be calculated from the mean thickness time dependence measurements made from the samples under treatment. These calculations were made for the treatments with each OCA in the following manner. From the VFs for natural tissue and knowing the natural sample volume, we calculated the absolute volumes for tissue components in natural sample. From sample thickness time dependence, we calculated the time dependence for sample volume. Since the absolute volume of scatterers is kept unchanged during treatment, we calculated scatterers' VF for any time of treatment by dividing the absolute volume by sample volume at different times of treatment. Since for any time of treatment the sum of VFs must equal unity (lower expression of Eq. (9)), we calculated the time dependence for the VF of ISF. Knowing the time dependence for the VFs in Eq. (9), the dispersion kinetics of the muscle could be calculated. Section 3 presents these results.

### 3 | RESULTS AND DISCUSSION

#### 3.1 | Muscle dispersion curve between 400 and 1000 nm

According to the methodology and tissue model that we described in section 2.3, to estimate muscle dispersion between 400 and 1000 nm, we need the dispersion of water and scatterers and corresponding VFs. Considering that all our measurements were performed at 20°C, we retrieved the RI data for water at this temperature from Ref. [28]. These data refer to wavelengths between 200 and 1130 nm and we have estimated the dispersion curve that fits the data in this range as:

$$n_{\text{water}}(\lambda) = \frac{p_1 \times \lambda^5 + p_2 \times \lambda^4 + p_3 \times \lambda^3 + p_4 \times \lambda^2 + p_5 \times \lambda + p_6}{\lambda^4 + q_1 \times \lambda^3 + q_2 \times \lambda^2 + q_3 \times \lambda + q_4}, \quad (10)$$

where  $p_1 = -2.577 \times 10^{-6}$ ,  $p_2 = 1.321$ ,  $p_3 = -176.2$ ,  $p_4 = 5.969$ ,  $p_5 = 0.4269$ ,  $p_6 = 0.5139$ ,  $q_1 = -138.2$ ,  $q_2 = -10.15$ ,  $q_3 = 0.1173$  and  $q_4 = 0.1223$ . The wavelength  $\lambda$  in Eq. (10) is to be used in nanometers. When performing the data fitting, using *cfitol* in MATLAB, we obtained an  $R^2$  value of 1. With the estimation of Eq. (10), the RI of water can be calculated for any particular wavelength to be used in the following calculations.

To calculate the dispersion for the dry proteins in muscle, we have collected the RI values of bovine muscle samples from Ref. [29]. These values correspond to wavelengths between 400 and 700 nm and are represented in Table 1:

We fitted the data in Table 1 with a curve described by Eq. (3) and extrapolated that curve to 1000 nm. When

TABLE 1 RI data between 400 and 700 nm for bovine muscle [29]

$\lambda$ (nm)	RI	$\lambda$ (nm)	RI
400	1.419	560	1.403
420	1.417	580	1.402
440	1.414	600	1.400
460	1.410	620	1.399
480	1.407	640	1.398
500	1.406	660	1.398
520	1.406	680	1.395
540	1.404	700	1.394

performing this fitting, we have obtained the following parameters in Eq. (3):  $A = 169.5$ ,  $B = 1.377$  and  $C = 1.374$  ( $R^2 = 0.985$ ). The data points in Table 1 and the fitting curve are presented in Figure 2.

The RI of bovine muscle at 589.6 nm was calculated with Eq. (3) as 1.400 and the RI of water was calculated with Eq. (10) as 1.333. Using these values and the RI of dry proteins (1.584) at the same wavelength in Eq. (4), we have calculated the VF for water in bovine muscle as 0.734. With all these values, we have determined the dispersion of dry proteins by subtracting the water contribution from the dispersion of bovine muscle. The resulting dispersion for the dry proteins is also presented in Figure 2. Using the dispersion curves of water (given by Eq. (10)) and dry proteins (orange curve in Figure 2) along with the corresponding VFs in rat muscle [27], we calculated the natural dispersion curve for skeletal muscle with Eq. (2). This curve is also presented in Figure 2 (red curve).

As indicated by the ovals and arrows, all data in Figure 2 are referred to the left vertical axis (in blue), with the exception of the orange curve, which is referred to the right vertical axis (in orange).

As presented in Figure 2, the RI of rat muscle at 589.6 nm is 1.398, the same as the mean of our previous measurements [2]. As a consequence of the decreasing behavior of water and dry proteins (see Eq. (10) and Figure 2), the RI of rat muscle also presents a decreasing behavior with wavelength. To compare this dispersion curve

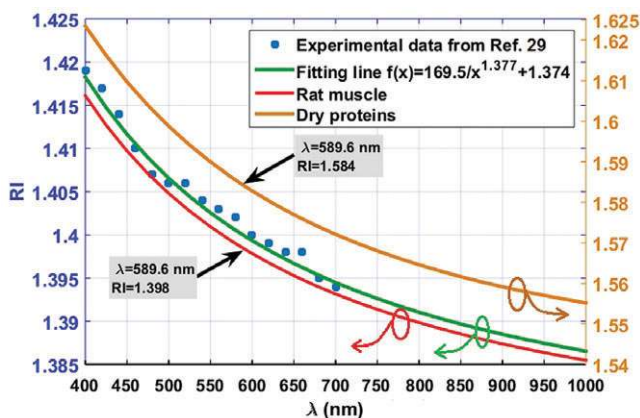


FIGURE 2 RI of skeletal muscle: Experimental data points for bovine (blue) [29], fitting curve (green), dry proteins (orange) and rat muscle (red)

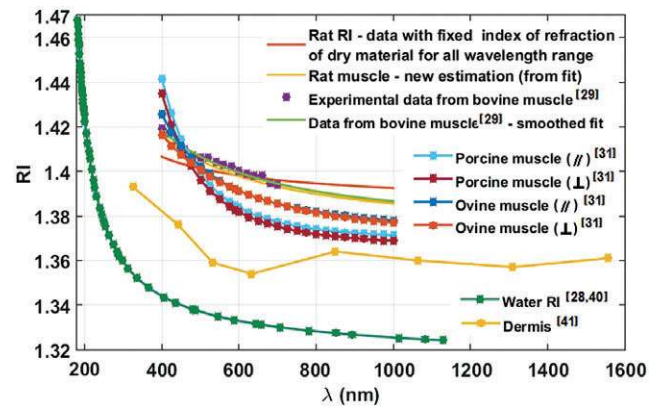


FIGURE 3 Wavelength dependence for water and tissue RI

with others from different tissues, we have created Figure 3 with data from several papers.

Figure 3 shows that although different values are seen for different tissues, all types of muscle present similar wavelength dependencies.

### 3.2 | Muscle dispersion kinetics during OC

To calculate muscle dispersion kinetics during OC, we started by determining the dispersion curve for scatterers with Eq. (5). This curve, which will remain unchanged during OC, is presented in Figure 4.

The data points in Figure 4 represent the calculated data for specific wavelengths: at each 25 nm between 400 and 1000 nm and for  $\lambda = 589.6$  nm for calculation control. The curve and points in Figure 4 were calculated using Eq. (5). The blue points are the RI values of the hydrated proteins that will be used in following calculations.

To obtain the dispersion kinetics for the interstitial space, we performed thickness and  $T_c$  measurements during the treatments with 40% glucose and 99% EG. Several muscle samples were prepared with circular form ( $\phi = 1$  cm) and 0.05 cm thickness to use in study. Considering the treatment with 40% glucose we used 3 samples to acquire time dependence thickness measurements and other 3 samples to acquire the  $T_c$  measurements during treatments.

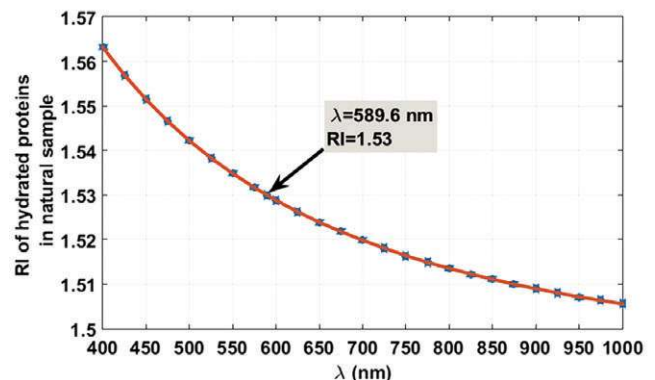


FIGURE 4 Wavelength dependence of the RI of hydrated proteins in rat skeletal muscle

Mean time dependence results were calculated both for sample thickness and  $T_c$ . A similar number of samples and procedure was used in the study with 99% EG. Mean total transmittance ( $T_t$ ) and total reflectance ( $R_t$ ) spectra of natural muscle were also calculated from individual measurements to be used in the kinetics calculations [33].

Considering the natural stage of muscle, we have performed 3 sets of Inverse Monte Carlo (IMC) and 3 sets of Inverse Adding-Doubling (IAD) simulations for several wavelengths between 400 and 1000 nm to estimate the optical properties. The IMC software code was created by our group, based on the forward Monte Carlo code developed by Lihong Wang and Steven Jacques and available at the website of the Oregon Medical Laser Center (<http://omlc.org/software/mc/>) [42]. The IAD software is the original code that was developed by Scott Prahl, also available at the website of the Oregon Medical Laser Center (<http://omlc.org/software/iad/index.html>) [43].

Thickness, optical measurements and the RI data presented in Figure 2 (red line) were used as input in these

simulations. Since both codes generated similar optical properties for all wavelengths considered in the simulations, the mean spectral optical properties of natural muscle were calculated between 400 and 1000 nm. These spectra are presented in Figure 5.

The points in graphs of Figure 5 represent the mean results of estimations using IMC and IAD simulations. The orange curves were created as interpolation between points to show that wavelength dependence of the optical properties are according to the literature— $\mu_a$  decreases with wavelength but shows an absorption peak around 500 to 550 nm due to the presence of hemoglobin in tissues;  $\mu_s$  decreases exponentially with wavelength and  $g$  increases exponentially with wavelength [7, 16].

Error bars in graphs (A) and (B) of Figure 5 are larger for smaller wavelengths, probably due to different blood content in samples used in measurements that were considered in the various simulations. For the case of anisotropy (Figure 5C), there is a higher uncertainty for all wavelengths considered, although the error bars are larger for

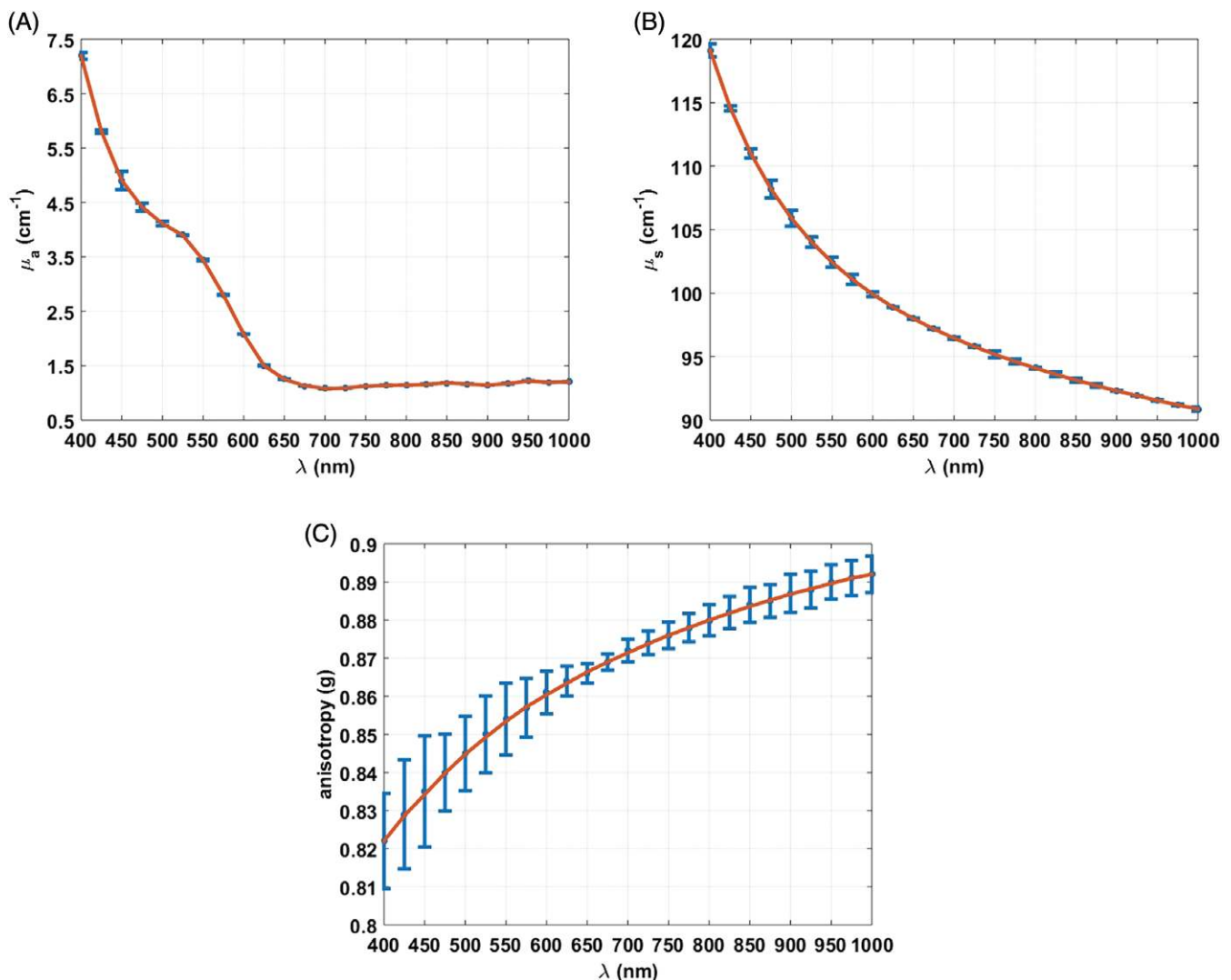


FIGURE 5 Mean optical properties of the skeletal muscle: (A) Absorption coefficient, (B) scattering coefficient and (C) scattering anisotropy factor

smaller wavelengths. This higher dispersion in estimated anisotropy values has to do with the low magnitude of the estimated values, which are smaller than 1.

The thickness time-dependent measurements were also used in these calculations. Mean results for these measurements obtained for the treatments with 40% glucose and 99% EG are presented in Figure 6 [9, 44], along with the  $T_c$  time dependence curves for some wavelengths from both studies.

The data presented in both graphs of Figure 6 represent mean results obtained from the measurements. For the case of thickness time dependence (Figure 6A), we have obtained higher uncertainty at the beginning, during the initial thickness decrease. For the treatment with EG, an uncertainty of 2.5  $\mu\text{m}$  was obtained at 15 and 30 seconds, decreasing later to a value of 0.5  $\mu\text{m}$ , which is maintained constant after 5 minutes of treatment. A similar uncertainty behavior was obtained for the thickness measurements during treatment with glucose solution. In this case, an uncertainty of 2.5  $\mu\text{m}$  was observed at 15 and 30 seconds, decreasing to a value of 0.5  $\mu\text{m}$  at 2 minutes, which is kept constant until 19 minutes. After 19 minutes of treatment, the uncertainty decreases to insignificant values. The reason for the higher uncertainty at the beginning of the treatment is that sample's compressibility is higher in natural state and during the dehydration mechanism. As the tissues lose water, the solid components approach each other and it is more difficult to compress the sample. For the  $T_c$  measurements made during both treatments, we observed a higher uncertainty of 0.0011% within the first 3 minutes of treatment. For later treatment, this uncertainty reduces to values as small as 0.0009%. Similar uncertainty values were observed in both treatments.

The mean thickness time dependencies for both treatments were used to calculate the VFs of hydrated proteins and interstitial space at any time of treatment. First, for natural tissue, we calculated the sample volume according to Eq. (11):

$$V_{\text{sample}} = (\pi \times 0.5^2) \times 0.05 = 3.927 \times 10^{-2} \text{ cm}^3 \quad (11)$$

Considering the skeletal muscle and according to Ref. [13], the VFs for free water are 0.1925 in the ISF and 0.4550 in sarcoplasm. Adding these values, we obtain a total free water content of 0.6475. Consequently, the VF of hydrated proteins (scatterers, or dry proteins plus bound water) is 0.3525. These values are reported in Ref. [13] for a study where rabbit, rat and frog muscle samples were used. In our case, we have used only rat skeletal muscle, meaning that we have to estimate the VFs for free water and hydrated proteins.

Using the RI of rat muscle that we have measured (1.398) [2], the RI of hydrated proteins (1.53) [37] and the RI of water (1.333) [28], all for 589.6 nm, in Eq. (2), we have estimated the VF for free water as 0.670. Also from Eq. (1), this value implies a VF of 0.330 for the hydrated proteins.

Multiplying these values by the sample volume given by Eq. (11), we calculated the absolute volumes for hydrated proteins and interstitial space plus sarcoplasm.

Using these values, we calculated the time dependence for the total volume of the sample from the time dependence of sample thickness. In these calculations, we considered Eq. (11), but replacing the natural thickness (0.05 cm) by the consecutive mean thickness values obtained for each treatment (presented in Figure 6A). Using the time dependence of sample's volume, we calculated the time dependence for the VF of hydrated proteins by dividing their absolute volume by the sample volume at each time of treatment. Since the sum of the partial volumes is always unity at any time of treatment, the VF of the interstitial space was obtained as the difference between unity and the VF of hydrated proteins. The results from these calculations are presented in Figure 7.

From the graphs in Figure 7, we see that VFs of tissue components suffer their higher magnitude variations during

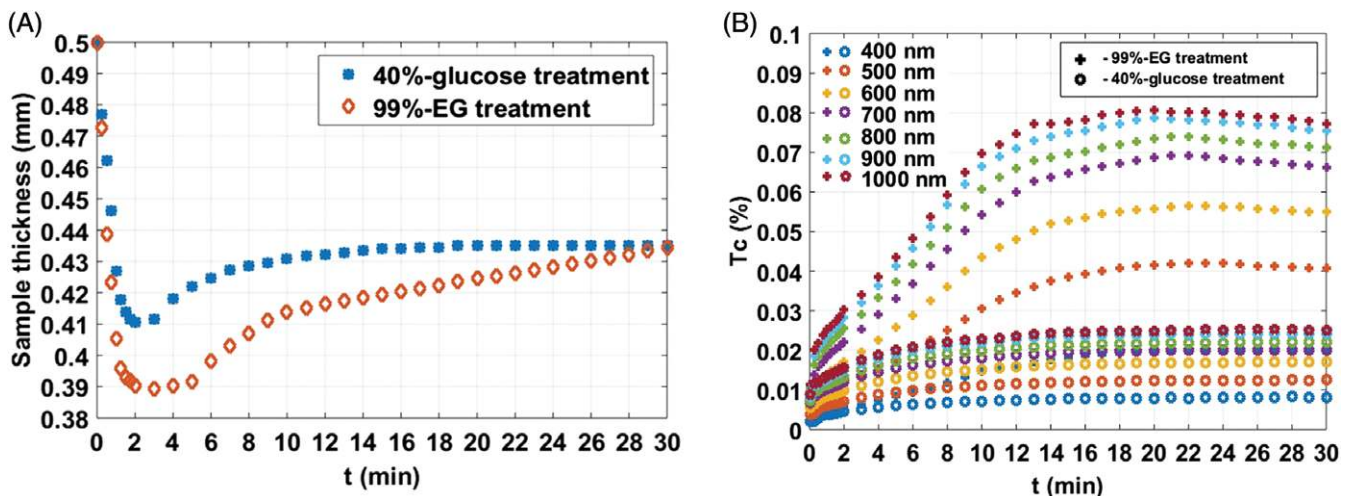


FIGURE 6 Mean time dependency measurements from samples under treatment with 40% glucose and 99% EG: (A) Sample thickness variation and (B)  $T_c$  at some wavelengths [12, 33, 34]



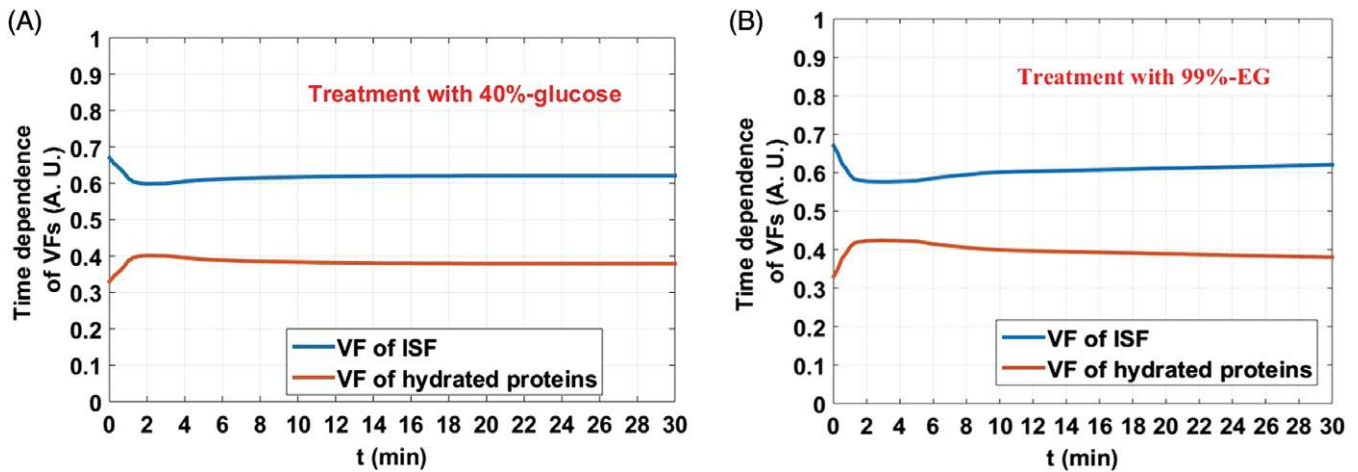


FIGURE 7 Time dependence of the VFs of tissue components during treatment with: (A) 40% glucose and (B) 99% EG

the first 10 minutes of treatment, before saturation regime is initiated. We also see that these variations are of higher magnitude for the treatment with EG. In both cases, we see that the hydrated proteins increase their VF during the first 3 minutes for both treatments. Such variation is related to the loss of water by the tissue. For the OCA to place itself near the muscle fibers to perform the RI matching mechanism at a latter stage of treatment, the water content in the interstitial space has to decrease at an early stage of treatment. Considering that free water exists both in sarcoplasm and in the ISF and since the OCA has to flow into the inside of the muscle cells, the free water in sarcoplasm has to flow into the interstitial space during dehydration. As we can see from the graph in Figure 7A, between approximately 6 and 18 minutes of treatment the VF of ISF plus sarcoplasm increases a little, indicating the inclusion of glucose to perform the RI matching. Such behavior is also seen for the treatment with EG between 6 minutes and the end of treatment (Figure 7B). It is important to understand that at the beginning of the treatment, when the dehydration mechanism dominates in OC, the major changes in the global RI

of the muscle will be driven by the variations in VFs presented in Figure 7. At later treatment, when RI matching becomes the dominant mechanism, the VFs do not show significant variations, as we can see from both graphs in Figure 7. At this later stage of the treatment, the driving force to produce variations in the sample's RI will be the change in the RI of ISF plus sarcoplasm, which is caused by the impregnation of these fluids with OCA.

To obtain this change in the RI of ISF plus sarcoplasm, we started by calculating the time dependence of the scattering coefficient through Eq. (7), from the thickness and  $T_c$  measurements made during treatments with both agents. In this calculation, we assumed that  $\mu_a$  remains constant during the treatments. Figure 8 presents the graphs for the time dependencies of  $\mu_t$  and  $\mu_s$  of the muscle for  $\lambda = 650$  nm.

Although the graphs in Figure 8 are relative only to 650 nm, similar calculations were performed for other wavelengths within 400 and 1000 nm. By comparing between both graphs in Figure 8, we see that EG originates a higher magnitude decrease in the attenuation and scattering coefficients than glucose. The first impact of the OCA

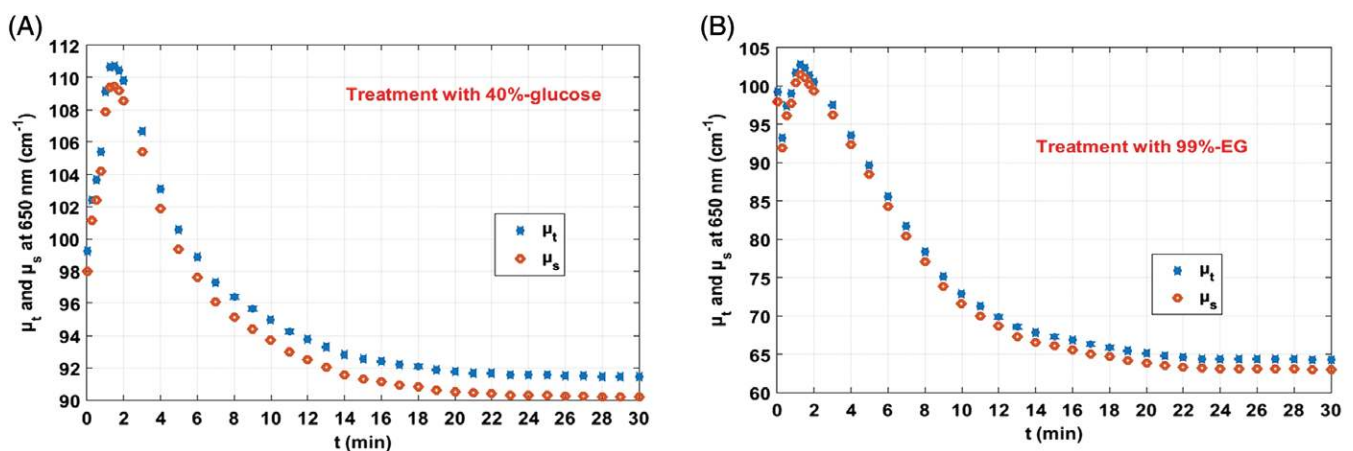


FIGURE 8 Time dependence for the attenuation and scattering coefficients of the muscle at 650 nm for the treatments with: (A) 40% glucose and (B) 99% EG

in solution is to increase both  $\mu_t$  and  $\mu_s$ . Due to the osmotic pressure of the OCA in the immersion solution, the dehydration mechanism is forced to initiate with the immersion of the sample in the solution. Consequently, as the water leaves the ISF to the outside, the muscle fiber cells will approach each other and such approach is translated by the initial increase in the coefficients that we see in both cases of Figure 8. In the treatment with EG, we see an initial decrease in the first 15 seconds of treatment. Such decrease might be explained by an early interaction of EG with superficial layers of the muscle sample. The global results seen in Figure 8 are a confirmation of our initial suspicion that OC produces a significant decrease in the scattering coefficient.

Using the time dependence of  $\mu_s$  along with thickness variations in Eq. (8), the time dependence of the RI of ISF plus sarcoplasm was calculated. Figure 9 presents the results of this calculation.

The graphs in Figure 9 show that the RI of ISF plus sarcoplasm increases during the treatments in a smooth manner. Although both OC mechanisms initiate at the beginning of treatment, the tissue dehydration mechanism dominates OC operations at the initial stage, while the RI matching mechanism dominates at longer treatment time. Considering the diffusion time values for water, glucose and EG in skeletal muscle that we have estimated in the diffusion study [12, 34], we can understand the variations presented in these graphs. In the diffusion studies, we estimated that the diffusion time in muscle is: 58 seconds for water [12, 34], 303 seconds for glucose [34] and 446 seconds for EG [12]. This means that with the immersion of the tissue in the treating solution, both the OC mechanisms begin immediately. Water begins to flow out of the tissue and OCA begins to flow in from the treating solution into the ISF and sarcoplasm. Considering the glucose treatment, graph in Figure 9A shows that the initial RI increase tends to saturate

at approximately 6 minutes. For the treatment with EG, we see from graph in Figure 9B that the initial RI increase tends to saturate at approximately 10 minutes. This extra time in the increase of the RI of the muscle fluids for the treatment with EG indicates that this OCA continues to flow into the sample for a longer time than glucose, but at the expense of sample thickness slight increase, as we have observed in Figure 6A.

From Figure 6A, we saw that both treatments produce strong decrease in tissue thickness at the early beginning of treatment, when tissue dehydration mechanism dominates over the RI matching. During the rest of the treatment, we see that RI follows the  $T_c$  behavior presented in Figure 6B. As usual, EG produces the higher magnitude variations in the RI of ISF plus sarcoplasm.

To finalize the study of muscle RI under treatment, we now present the results of the dispersion kinetics for the whole muscle, as calculated with Eq. (9) for each time of treatment. In these calculations, we added the contributions of tissue scatterers and fluids. The appropriate VFs for both treatments that are represented in the graphs of Figure 7 were used in these calculations. The dispersion kinetics of muscle during both treatments is presented in Figure 10.

Both graphs in Figure 10 show an initial strong increase in muscle's RI, although EG produces the higher magnitude increase. As indicated in the color bars of the graphs in Figure 10, this initial increase in RI corresponds to the treatment time period where the dehydration mechanism dominates OC operations. After the initial increase, there is a transition period where both OC mechanisms occur simultaneously. Later, during treatment, the sample's RI tends smoothly to become stable. During this period, the RI matching mechanism dominates OC operations.

This behavior is an evidence of the 2 OC mechanisms: tissue dehydration at the beginning and RI matching later

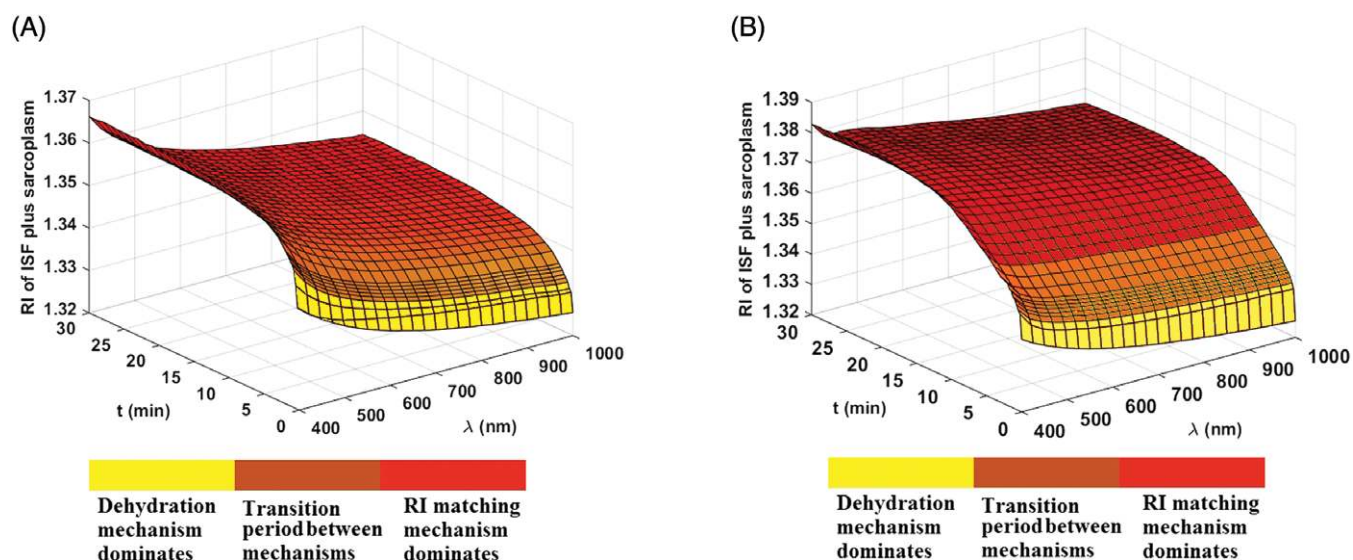


FIGURE 9 Time dependence for the RI of sarcoplasm plus ISF for the treatments with: (A) 40% glucose and (B) 99% EG

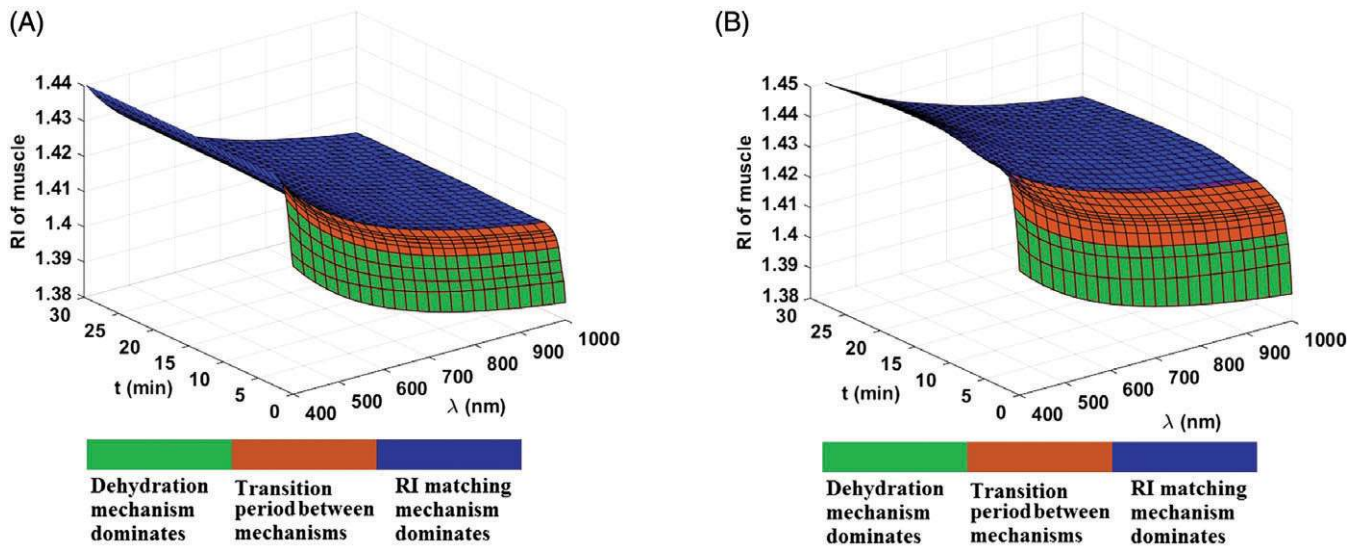


FIGURE 10 Time dependence of the RI of muscle for treatments with: (A) 40% glucose and (B) 99% EG

on. Comparing between the graphs in Figure 10, we see that the final values of muscle RI are higher for the treatment with EG. Such difference is seen for the entire spectral range.

The second difference is that the sample treated with EG presents a rising behavior for the RI that lasts longer than in the treatment with glucose. Such differences are related to the different OCA concentrations used in both treatments. At the end of the treatment with EG, we see a little decrease in the RI values, just as we saw from the  $T_c$  time dependence for that treatment (Figure 6B) [33]. Such differences in the time dependence of the sample's RI correlate well to the experimental measurements that have originated them: thickness and  $T_c$  time dependencies; and these measurements are sensitive enough to evaluate RI changes in the interstitial space according to the theoretical model we used.

Such theoretical model, which is based only on thickness and  $T_c$  experimental measurements demonstrates the occurrence of the RI matching mechanism. The calculations made with the proposed algorithm were only possible assuming that  $\mu_a$  is much smaller than  $\mu_s$ . Fortunately, not only the skeletal muscle, but the great majority of soft tissues also has this characteristic and the model used is adequate to perform such calculations. By performing these measurements during OC treatments, we were able to observe an increase in the spectral RI of the muscle fluids (Figure 9), meaning that the RI mismatch decreased its magnitude during treatments. Such decrease corresponds to a decrease in tissue scattering. By evaluating the RI time dependence for a spectral range between UV and NIR wavelengths, it was verified that the partial replacement of tissue water by the OCAs produces similar efficiency in the entire range, provided that no strong absorption bands exist.

Comparing between the results obtained from the treatments with the 2 OCAs (the graphs of Figures 9 and 10),

we see that EG produces a higher magnitude RI matching between tissue components, meaning that the method used in our research is sensitive enough to be used in different OC treatments and with different OCAs. Further processing of the time dependencies obtained in this study can be used to establish quantification parameters for the RI matching mechanism and OC efficiency. Such information is of great importance if the optimization of OC treatments in clinical practice is an objective.

#### 4 | CONCLUSIONS

We have observed that the proposed indirect method is very sensitive to the time dependence of  $n_0$ . The results of the calculations made for various wavelengths between 400 and 1000 nm show indeed that the RI of the interstitial space increases during treatment. These results prove the occurrence of the RI matching mechanism and the simple calculation method, which is based only on  $T_c$  and thickness measurements, can now be used to perform similar evaluations on other tissues and OC treatments.

Once the dispersion kinetics are calculated for the skeletal muscle with these OCAs, the kinetics of the optical properties can also be estimated through IMC simulations, provided that integrated optical transmittance and reflectance measurements are made on similar conditions. The evaluation of the time dependency of the optical properties will allow the evaluation of OC efficiency. We plan to perform these studies briefly.

#### ACKNOWLEDGMENT

For the preparation of biological samples, the authors would like to thank to LAIMM—Laboratory of Support to


Research in Molecular Medicine from the Department of Experimental Biology, Faculty of Medicine, University of Porto, Porto, Portugal. This work was supported by the Government of Russian Federation (grant 074-U01), Russian Presidential grant NSh-7898.2016.2, and RFBR grant 17-02-00358.

## AUTHOR BIOGRAPHIES

Please see Supporting Information online.

## ORCID

Luís M. Oliveira  <http://orcid.org/0000-0003-0667-3428>

Valery V. Tuchin  <http://orcid.org/0000-0001-7479-2694>

## REFERENCES

- [1] V. V. Tuchin, *Optical Clearing of Tissues and Blood*, SPIE Press, Bellingham, WA **2006**, p. 1.
- [2] L. Oliveira, A. Lage, M. Pais Clemente, V. V. Tuchin, *Opt. Lasers Eng.* **2009**, *47*, 6.
- [3] L. Oliveira, A. Lage, M. Pais Clemente, V. V. Tuchin, *J. Biomed. Opt.* **2010**, *15*, 5.
- [4] V. V. Tuchin, *Tissue Optics: Light Scattering Methods and Instruments for Medical Diagnosis*, 3rd ed., SPIE Press, Bellingham, WA **2015**, p. 3.
- [5] W. Cheong, S. A. Prael, A. J. Welch, *IEEE J. Quant. Electron.* **1990**, *26*, 12.
- [6] A. N. Bashkatov, E. A. Genina, V. V. Tuchin, *J. Innov. Opt. Health Sci.* **2011**, *4*, 1.
- [7] S. L. Jacques, *Phys. Med. Biol.* **2013**, *58*, 11.
- [8] J. Mobley, T. Vo-Dinh, V. V. Tuchin, in *Biomedical Photonics Handbook* (Ed: T. Vo-Dinh), CRC Press LLC, Boca Raton, FL **2015** Ch. 2.
- [9] L. Oliveira, M. Inês Carvalho, E. Nogueira, V. V. Tuchin, *J. Innov. Opt. Health Sci.* **2016**, *9*, 5.
- [10] E. A. Genina, A. N. Bashkatov, V. V. Tuchin, *Expert Rev. Med. Devices* **2010**, *7*, 6.
- [11] L. Oliveira, *Ph.D. Thesis*, Porto University (Portugal), November **2014**.
- [12] L. Oliveira, M. I. Carvalho, E. Nogueira, V. V. Tuchin, *J. Biomed. Opt.* **2015**, *20*, 5.
- [13] R. C. Haskell, F. D. Carlson, P. S. Blank, *Biophys. J.* **1989**, *56*, 2.
- [14] A. N. Bashkatov, E. A. Genina, V. I. Kochubey, V. S. Rubtsov, E. A. Kolesnikova, V. V. Tuchin, *Quant. Electron.* **2014**, *44*, 8.
- [15] S. Carvalho, N. Gueiral, E. Nogueira, R. Henrique, L. Oliveira, V. V. Tuchin, in *Dynamics and Fluctuations in Biomedical Photonics XIV*. Proc. SPIE 10063 (Eds: V. V. Tuchin, K. V. Larin, M. J. Leahy, R. K. Wang), SPIE - the international society for optics and photonics, San Francisco, CA **2017**, p. 100631L-1-16.
- [16] A. N. Bashkatov, E. A. Genina, V. I. Kochubey, V. V. Tuchin, *J. Phys. D: Appl. Phys.* **2005**, *38*, 15, 2543.
- [17] T. L. Troy, D. L. Page, E. M. Sevick-Muraca, *J. Biomed. Opt.* **1996**, *1*, 3.
- [18] V. G. Peters, D. R. Wyman, M. S. Patterson, G. L. Frank, *Phys. Med. Biol.* **1990**, *35*, 9.
- [19] M. C. Meinke, M. Friebe, J. Helfmann, in *Advanced Optical Flow Cytometry: Methods and Disease Diagnosis* (Ed: V. V. Tuchin), Wiley-VCH, Weinheim, Germany **2011** Ch. 5.
- [20] M. Meinke, G. Müller, J. Helfmann, M. Friebe, *Appl. Opt.* **2007**, *46*, 10.
- [21] R. Cicchi, F. S. Pavone, D. Massi, D. D. Sampson, *Opt. Express* **2005**, *13*, 7.
- [22] X. Wen, S. L. Jacques, V. V. Tuchin, D. Zhu, *J. Biomed. Opt.* **2012**, *17*, 6.
- [23] D. W. Leonard, K. M. Meek, *Biophys. J.* **1997**, *72*, 3.
- [24] K. M. Meek, S. Dennis, S. Khan, *Biophys. J.* **2003**, *85*, 4.
- [25] K. M. Meek, D. W. Leonard, C. J. Connon, S. Dennis, S. Khan, *Eye* **2003**, *17*, 8.
- [26] O. Zhemovaya, O. Sydoruk, V. Tuchin, A. Douplik, *Phys. Med. Biol.* **2011**, *56*, 13.
- [27] R. F. Reinoso, B. A. Telfer, M. Rowland, *J. Pharmacol. Toxicol. Methods* **1997**, *38*, 2.
- [28] M. Daimon, A. Masumura, *Appl. Opt.* **2007**, *46*, 18.
- [29] F. P. Bolin, L. E. Preuss, R. C. Taylor, R. J. Ference, *Appl. Opt.* **1989**, *28*, 12.
- [30] A. Douplik, G. Saiko, I. Schelkanova, V. V. Tuchin, in *Lasers for Medical Applications: Diagnosis, Therapy and Surgery* (Ed: H. Jelinkova), Woodhead Publishing Ltd, Prague, Czech Republic **2013** Ch. 3.
- [31] S. Cheng, H. Y. Shen, G. Zhang, C. H. Huang, X. J. Huang, in *Light Tissue Interaction II*. Proc. SPIE 4916 (Eds: B. Chance, M. Chen, G. Yoon), SPIE - the international society for optics and photonics Shanghai, China **2002**, p. 172.
- [32] A. S. Ginzburg, M. A. Gromov, G. I. Krasovskaya, *Handbook on Thermophysical Characteristics of Food Products*, Agropromizdat, Moscow, Russia **1990**.
- [33] L. Oliveira, M. Inês Carvalho, E. Nogueira, V. V. Tuchin, *J. Innov. Opt. Health Sci.* **2013**, *6*, 2.
- [34] L. Oliveira, M. I. Carvalho, E. Nogueira, V. V. Tuchin, *Laser Phys.* **2013**, *23*, 7.
- [35] V. Gillard, R. Martino, M. Malet-Martino, M. Riviere, A. Gournay, R. Navarro, *Int. J. Cosmet. Sci.* **1998**, *20*, 2.
- [36] B. Schultz, D. Chan, J. Bäckström, M. Rübhausen, *Thin Solid Films* **2004**, *455*, 731.
- [37] W. L. Bragg, A. B. Pippard, *Acta Crystallogr.* **1953**, *6*.
- [38] T. Yu, X. Wen, V. V. Tuchin, Q. Luo, D. Zhu, *J. Biomed. Opt.* **2011**, *16*, 9.
- [39] M. Rinehart, H. S. Park, K. A. Walzer, J.-T. A. Chi, A. Wax, *Sci. Rep.* **2016**, *6*.
- [40] G. M. Hale, M. R. Querry, *Appl. Opt.* **1973**, *12*, 3.
- [41] X. Ma, J. Q. Lu, H. Ding, X.-H. Hu, *Opt. Lett.* **2005**, *30*, 4.
- [42] L. Wang, S. L. Jacques, L. Zheng, *Comput. Methods Programs Biomed.* **1995**, *47*(2).
- [43] S. A. Prael, M. C. van Gemert, A. J. Welch, *Appl. Opt.* **1993**, *32*, 4.
- [44] P. Peixoto, L. Oliveira, M. Inês Carvalho, E. Nogueira, V. V. Tuchin, *J. Biomed. Photon. Eng.* **2016**, *1*, 4.

**How to cite this article:** Oliveira Luís M., Carvalho MI, Nogueira EM, Tuchin VV. Skeletal muscle dispersion (400-1000 nm) and kinetics at optical clearing. *J. Biophotonics*. 2017;e201700094. <https://doi.org/10.1002/jbio.201700094>